

RESEARCH ARTICLE | APRIL 21 2022

Analysis of turbulence generation and dissipation in shear layers of methane–oxygen diffusion flames using direct numerical simulations

Daniel Martinez-Sanchis  ; Sagnik Banik ; Andrej Sternin ; Daniel Sternin; Oskar Haidn; Martin Tajmar 



Physics of Fluids 34, 045121 (2022)

<https://doi.org/10.1063/5.0087887>



Physics of Fluids

Special Topic: K. R. Sreenivasan:
A Tribute on the occasion of his 75th Birthday

Submit Today

 AIP
Publishing

Analysis of turbulence generation and dissipation in shear layers of methane–oxygen diffusion flames using direct numerical simulations

Cite as: Phys. Fluids **34**, 045121 (2022); doi: 10.1063/5.0087887

Submitted: 10 February 2022 · Accepted: 1 April 2022 ·

Published Online: 21 April 2022



View Online



Export Citation



CrossMark

Daniel Martinez-Sanchis,^{1,a)}  Sagnik Banik,¹  Andrej Sternin,^{1,2}  Daniel Sternin,¹ Oskar Haidn,¹ and Martin Tajmar² 

AFFILIATIONS

¹Chair of Space Propulsion Technische, Universität München, Boltzmannstraße 15, Garching, Germany

²Chair of Space Systems/Technische, Universität Dresden, Marschnerstraße 32, Dresden, Germany

^{a)}Author to whom correspondence should be addressed: daniel.martinez@tum.de

ABSTRACT

A turbulent methane–oxygen diffusion flame is studied using a direct numerical simulation setup. The operating regime and turbulence characteristics are chosen to resemble those of a modern methane rocket combustor. Local flame characteristics and dimensionless numbers are defined and evaluated, and their relationship with the turbulent kinetic energy transport budget is studied. Positive net turbulence generation is observed in the reaction shear layer. It is found that the underlying mechanisms for these results are similar to those encountered in premixed flames, with pressure terms acting as the primary turbulent kinetic energy sources. Models for predicting turbulent transport through mean pressure gradients, fluctuating pressure gradients, and turbulent flux of turbulent kinetic energy are adapted. The accuracy of the proposed formulations is assessed, and the involved challenges are discussed.

© 2022 Author(s). All article content, except where otherwise noted, is licensed under a Creative Commons Attribution (CC BY) license (<http://creativecommons.org/licenses/by/4.0/>). <https://doi.org/10.1063/5.0087887>

I. INTRODUCTION

Technical combustion applications operate nearly always in turbulent conditions. The chemical changes associated with the reactants' burning pose a significant challenge to the predictability of the flow statistics. Changes in viscosity and density can be above one order of magnitude. These variations activate additional vorticity and turbulence transport mechanisms, which lead to significant deviations from the standard models. Depending on the context, the integral result of these effects can be the promotion or suppression of turbulence.

Karlovitz *et al.*¹ noticed turbulence generation associated with combustion in premixed regimes. Global creation of turbulence in premixed flames was repeatedly observed in subsequent experiments during the following years.^{2–5} The overall generation/destruction of turbulence originates from several individual processes that emerge from the celebrated Navier–Stokes equations. Understanding their distinctive behavior is necessary to approach modeling of the combustion influence on the turbulence statistics. Although global turbulence transport can be evaluated experimentally in specific environments, quantifying all the involved sources poses a prohibitively expensive and complex challenge. Due to this limitation, the underlying physical

motivations behind turbulent transport in premixed combustion remained veiled for several years.

Thanks to the increase in computational power, direct numerical simulations (DNS) of turbulent flames with a reasonable number of simplifications became affordable at the end of the 20th century. The accuracy of these simulations is unrivaled, providing unique insights that can be used to develop and validate statistical models. The pioneering work of Rutland and Cant⁶ paved the way to the detailed study of turbulence transport in premixed flames resorting to numerical simulations. DNS results have been used ever since as a tool to fathom turbulence and vorticity transport processes in a combusting flow. The ultimate goal of such research is to model the unknown terms in the Reynolds-averaged conservation equations to achieve closure. However, progress in modeling the coupling between turbulence and chemistry in premixed flames is relatively moderate, as reviewed elsewhere.^{7,8} Despite this lack of completeness, several consistent trends have been observed, which are useful for understanding the ongoing interactions. The relationship between chemical and turbulent scales has proven to be a solid indicator of how combustion can influence turbulence. In this frame, the Damköhler and Karlovitz numbers have

been revealed as robust parameters to predict whether combustion will annihilate or create turbulence. On a superficial level, it can be summarized that if chemical processes are fast and small compared to turbulence (high Da and low Ka), turbulence generation can be expected. A more detailed explanation of these effects can be found in the works by Chakraborty.^{9,10}

Due to their conceptual simplicity, premixed flames are a suitable foundation for addressing the question of in-flame turbulence generation. However, most engines operate under non-premixed conditions. In such a context, fuel and oxidizer are injected separately, and they must meet to enable the progress of chemical reactions. The development of these flames is driven by mass and heat diffusion processes. Non-premixed combustion introduces further levels of complexity compared to their premixed counterparts. Chemical scales are no longer static properties but vary in space depending on the local mixing. Non-premixed flames depend on the injection setup, and the turbulence statistics are transported in at least two directions. This implies a substantial complexity enhancement compared with the premixed flames, whose development is essentially unidimensional. Consequently, simulations must run over more extended periods of time to achieve ergodicity in the flow statistics. Due to these challenges, the study of turbulent transport in non-premixed combustion using DNS is rather scarce.

In high-pressure applications, such as the injection system of a rocket engine, the chemical length scales experience extreme gradients due to the complex chemistry and mixing processes. These intricate phenomena can trigger a wide variety of unexplored flame-vortex dynamics, which conventional models are unable to capture. The design of rocket combustion chambers is constrained in one way or another by the limited understanding of these processes. Enhancing knowledge in this field is a critical step in developing more efficient systems, achieving high characteristic velocities with minimal length.^{11–13} The present work investigates turbulence transport in such a combustion context. Direct numerical simulations are used to investigate the interactions between chemistry and combustion in a co-flow methane–oxygen diffusion flame. The turbulence characteristics are chosen to resemble the ones expected in the injection region of a rocket combustor. The characteristic time and length scales of turbulence and combustion are evaluated through the flame, and local Damköhler and Karlovitz numbers are measured. These results are subsequently compared with the turbulent kinetic energy budget to examine the different sources and sinks of turbulence along with the flame.

The rest of the paper is structured as follows. Section II provides the necessary theoretical background to evaluate the problem of turbulent transport in the context of a diffusion flame. This introduction is followed by a detailed description of the simulation setup and the post-processing strategies. The simulation output will be subsequently described, and the results of the flow’s statistical analysis discussed. In the end, final remarks are provided, summarizing the identified phenomena and further challenges.

II. THEORETICAL BACKGROUND

It is convenient to reprise certain basic concepts before discussing in detail the simulation results. First, we shall present the characteristic scales of turbulence. This introduction is followed by the presentation of the turbulent kinetic energy transport equation, including a brief discussion on the main sources and sinks, along with their physical implications. The most relevant chemical parameters and scales are

subsequently introduced to enable the comparison with the turbulent processes.

A. Turbulence characterization

Turbulent flows are chaotic by definition.^{14,15} Hence, it is unrealistic to attempt the exact calculation of properties and trajectories for every point in the domain as a function of time. Instead, a stochastic approach is deemed more suitable. The most relevant statistical parameter of a quantity q is its time average $\bar{q} = (1/t_{end}) \int_0^{t_{end}} q(t) dt$. This mean value is referred to as Reynolds average, and it is a central concept in the characterization and modeling of turbulent flows. In flows with relevant variations in specific volume, filtering instantaneous values with density provides a more compact formulation. This notion leads to the Favre average,¹⁶ which is defined as follows:

$$\tilde{q} = \frac{1}{\bar{\rho} t_{end}} \int_0^{t_{end}} \rho(t) q(t) dt. \quad (1)$$

Taking this value as reference, it is possible to define a Favre fluctuation $q''(t)$ as the instantaneous deviation from the expected mean value, i.e., $q''(t) = q(t) - \tilde{q}$. The properties of fluctuations are essential in the characterization of the flow’s behavior. By definition, averaged fluctuations are zero, i.e., $\tilde{q}'' = 0$. Hence, it is necessary to consider higher-order statistics to address their analysis. The most direct indicator is the second-order moment, i.e., q''^2 , which is denoted as the variance. The variance of velocity fluctuations is the basis for the turbulent kinetic energy definition,

$$\tilde{k}_i = \frac{\overline{\rho u_i'' u_i''}}{2\bar{\rho}}. \quad (2)$$

This parameter is of ultimate relevance since it is directly coupled with average properties through the momentum conservation equations. Isotropy in (2), i.e., $\tilde{k}_1 = \tilde{k}_2 = \tilde{k}_3$, is a common assumption in classical turbulence theory. Nevertheless, turbulent flames are highly anisotropic as most of the turbulent kinetic energy tends to concentrate in the main flow propagation direction.^{17,18}

The turbulent kinetic energy constitutes an integral quantity. This value results from the superposition of a wide number of eddies or vortices, which are moving topologies whose turbulent fluctuations exhibit a certain degree of coherence. These vortical structures are characterized by their individual size or length scale. The different eddy scales are central in understanding the interactions between turbulence and combustion. Depending on their overlap with their chemical counterparts, turbulent and combustion processes will influence each other in one direction or another.¹⁹ The most relevant length scales for understanding these interactions are presented in this section.

The size of the largest eddies can be estimated as follows:²⁰

$$\tilde{L} = \sqrt{\tilde{k}^3 / \tilde{\epsilon}}, \quad (3)$$

where $\tilde{\epsilon}$ is the Favre-averaged turbulent kinetic energy dissipation rate, which is defined as follows:

$$\tilde{\epsilon} = \mu \left(\frac{\partial u_i''}{\partial x_j} \frac{\partial u_i''}{\partial x_j} \right) / \bar{\rho}. \quad (4)$$

This parameter represents one of the leading turbulent kinetic energy sinks, and it accounts for the dissipation of vortical structures due to viscous effects. This parameter can be used to estimate the characteristic timescale of the large eddies as follows:

$$t_T = \tilde{k} / \tilde{\varepsilon}. \tag{5}$$

Finally, the size of the smallest eddies shall be commented. This length is often referred to as the Kolmogorov scale, and it can be estimated as a function of the viscosity and the dissipation rate,

$$\tilde{\eta} = \left(\frac{(\tilde{\mu} / \tilde{\rho})^3}{\tilde{\varepsilon}} \right)^{1/4} = \left(\frac{\tilde{\nu}^3}{\tilde{\varepsilon}} \right)^{1/4}. \tag{6}$$

The discussed eddy sizes are particularly relevant in the frame of scale-resolving simulations since they are tightly coupled with the resolution requirements. The large-eddy scale provides a lower bound of the necessary domain size to achieve statistical convergence. In particular, a domain size $L_p \geq 8\tilde{\Lambda} \approx 4\tilde{L}$ is recommended by Pope in DNS,²¹ with $\tilde{\Lambda}$ being the integral eddy length. In addition, the Kolmogorov scale determines the maximum cell grid size $\Delta x_{max} \approx 2.1\eta$.²² Larger cells might require sub-grid scale models to account for the non-resolved turbulent kinetic energy.

B. Transport of turbulent kinetic energy

Determining the spatial-temporal evolution of the turbulent kinetic energy is a core problem in turbulent flows. The turbulence development is governed by the turbulent kinetic energy transport equation which originates from the Navier–Stokes conservation equations. For the case of Favre-averaged turbulent kinetic energy, it can be expressed as follows:^{9,23,24}

$$\begin{aligned} \frac{\partial \tilde{\rho} \tilde{k}}{\partial t} + \frac{\partial \tilde{\rho} \tilde{u}_j \tilde{k}}{\partial x_j} = & \underbrace{-\overline{\rho u_i'' u_j''}}_{T_1} \frac{\partial \tilde{u}_i}{\partial x_j} - \underbrace{u_i'' \frac{\partial \tilde{p}}{\partial x_i}}_{T_2} + \underbrace{p' \frac{\partial u_k''}{\partial x_k}}_{T_3} + \underbrace{u_i'' \frac{\partial \tau_{ij}}{\partial x_j}}_{T_4} \\ & - \underbrace{\frac{\partial p' u_i''}{\partial x_i}}_{T_5} - \underbrace{\frac{\partial}{\partial x_i} \left(\frac{1}{2} \overline{\rho u_i'' u_k'' u_k''} \right)}_{T_6}. \end{aligned} \tag{7}$$

Most of the elements on the right-hand side of (7) are unclosed, and modeling is required for their determination. Predicting these terms through the mean flame brush has been subject of intense research during the last decades. The most unified approach is the procedure proposed by Bray *et al.*,²⁵ also called the Bray–Moss–Libby (BML) method. In addition, several works have addressed the modeling of single elements in (7) using empirical approaches. The challenges involved in modeling each of these terms are briefly reviewed in the text below.

The term T_1 represents the turbulent production through mean velocity gradients. This naming can be misleading in the present context since it naturally tends to destroy turbulence. This behavior can be easily elucidated if we consider a statistically planar flame that accelerates in a main direction x_1 as combustion progresses. Since $\overline{\rho u_1'' u_1''}$ and the velocity gradients along the mean flame brush are positive, T_1 presents negative values overall. In the context of isotropic turbulence, T_1 is closed, and no modeling is required. This is not the case in turbulent flames, which are highly anisotropic flows. In this sort of context,

the turbulent kinetic energy tends to concentrate in the main flow propagation direction.^{17,18} Several approaches have been proposed to model the anisotropic behavior of the Reynolds stress tensor (RST) $\overline{\rho u_i'' u_j''}$. The simplest models are based on the kinematic eddy viscosity ν_T .^{26–28} The BML model allows to predict the Reynolds stress tensor as well, and it can be used to close T_1 . Chakraborty *et al.*⁹ compared the performance of these different methodologies over various regimes. The BML method exhibited a better agreement with numerical simulations regardless of the combustion regime. Eddy viscosity models performed fairly well at moderate to high Karlovitz numbers, but the agreement with observed DNS statistics worsened as the Karlovitz number decreased.

The term T_2 represents the turbulence generation through mean pressure gradients. This term was identified as one of the primary sources of flame-generated turbulence.^{23,24} Nishiki *et al.*²⁴ modeled the unclosed part of this term, i.e., $\overline{u_i''}$ in the frame of premixed flames. Their model has presented excellent agreement with the observed results,^{9,29} but it requires additional modeling of the turbulent scalar flux $\overline{\rho u_i'' c''}$, which has been addressed in other research.^{30–34}

The terms T_3 and T_5 are easier to approach if both are considered together as the pressure fluctuations gradients as follows:

$$T_{FPG} = T_3 + T_5 = \overline{u_k'' \frac{\partial p'}{\partial x_k}}. \tag{8}$$

This term is one of the main turbulence sources in premixed turbulent flames.^{9,23,24,29} Several empirical models have been proposed for T_{FPG} .^{23,35,36} Nevertheless, their performance is susceptible to the different combustion regimes.⁹ Recent research indicates that it can be possible to model T_{FPG} through the flame curvature,³⁷ although the validity of this approach is conditioned to the dominant diffusion processes ($Le \geq 1$).

The term T_4 describes molecular diffusion and viscous dissipation, and it is primarily analogous to the concept of dissipation rate. This term can be recast as follows:

$$\begin{aligned} T_4 = & -\overline{\rho \tilde{\varepsilon}} + \underbrace{\left(u_i'' \frac{\partial}{\partial x_k} \left(\mu \frac{\partial u_k}{\partial x_i} \right) - \frac{2}{3} u_i'' \frac{\partial}{\partial x_j} \left(\mu \frac{\partial u_k}{\partial x_k} \right) \right)}_{T_V} \\ & + \frac{\partial}{\partial x_j} \left(\mu \frac{\partial \tilde{k}}{\partial x_j} \right). \end{aligned} \tag{9}$$

In general, it can be taken $T_4 \approx -\overline{\rho \tilde{\varepsilon}}$ since dissipation dominates the other two terms in (9). The dissipation rate has its own transport equation in the frame of $k - \varepsilon$ modeling. The last term in (9), i.e., $\nabla \cdot (\mu \nabla \tilde{k})$ represents the molecular viscous transport and is closed. Hence, T_V is the only term whose modeling shall be addressed. This term presents mostly a negative value, although its influence in turbulent premixed flames is negligible when compared with $\overline{\rho \tilde{\varepsilon}}$. Efforts to model T_V based on empirical assumptions were conducted by Nishiki *et al.*²⁴ and Chakraborty *et al.*⁹ The proposed models are able to consistently capture the overall behavior through the flame brush.

In turbulent premixed flames, the term T_6 acts mainly as a source, and it is among the main responsible sources for turbulence generation in low Karlovitz number regimes. This element's modeling is rendered as complex since it depends on the statistic $\overline{\rho u_i'' u_k'' u_k''}$, which is challenging to address. This parameter can be estimated

following the BML method as described by Chakraborty *et al.*⁹ Nevertheless, the prediction capabilities of this approach in terms of turbulent transport are limited.

C. Chemistry characterization

The characterization of chemical processes requires the determination their length and time scales. These values enable a comparison with the previously discussed turbulent quantities. The deduction of chemical scales is particularly challenging in the frame of non-premixed combustion.³⁸ Most premixed flames can be considered stochastically planar,⁹ meaning that the statistical properties are constant in the surface, normal to the main flame propagation's direction. In diffusion flames, however, the progress of chemistry is strongly conditioned to the local mixing. This feature increases the problem's complexity by adding additional degrees of freedom. Consequently, chemical scales must be studied as a function of space to capture local variations associated with the mixing development. This section is devoted to discussing the most relevant elements in the characterization of turbulent diffusion flames. One of the main goals in the present work is to investigate the interactions between combustion and the integral turbulence statistics. With this aim in mind, the presented definitions were chosen to be dependent on data that is usually accessible within the frame Reynolds-averaged Navier–Stokes (RANS) models. This constraint will ease the applicability of the derived expressions, although some preciseness might be lost. The validity of these simplifications within the performed simulations is briefly commented to justify its legitimacy.

1. Progress variable c

The progress variable c is a dimensionless indicator that represents the combustion process development ranging from zero to unity. The most common definition of the progress variable has the following form:³⁹

$$c = \frac{q - q_R}{q_P - q_R}, \quad (10)$$

where q is a quantity representative of the overall combustion process evolution. The subscripts R and P stand for “reactants” and “products,” respectively. One core requirement of such a quantity is presenting a monotonic trend through the flame.⁴⁰ Temperature, species concentration, or density are common examples of quantities used to define the progress variable in premixed combustion. In a diffusion flame, none of these parameters alone suffices to assess the local flame evolution since their value is not solely dependent on the combustion development. For example, the temperature at a given point can be originated from the exothermic chemical reactions or from the heat transfer of hot products in the vicinity. Furthermore, the introduction of detailed chemistry can alter the monotonic behavior of certain quantities⁴⁰ or their linearity.⁴¹ To counter this sort of issues, more sophisticated definitions are required. The expression in (10) can be written in a more generalized way as proposed by Bray *et al.* as follows:⁴²

$$c = \frac{Y_c}{Y_c^{Eq}(Z)}, \quad (11)$$

where Y_c is the reaction progress variable and Z is the mixture fraction.^{43,44} The mixture fraction is a quantity denoting the combined

mass fractions of hydrogen and carbon atoms. Hence, it tends to unity toward the fuel side and to zero in the oxidizer region. $Y_c^{Eq}(Z)$ denotes the equilibrium reaction progress in a given mixture fraction. The reaction progress Y_c is an expression that aims at summarizing the local development of the combustion process. This is often achieved through the combination of species or relevant parameters. One common approach is to consider the addition of the most significant final products. Pierce and Moin⁴⁵ suggested the following formulations in the frame of non-premixed Methane combustion:

$$Y_{c_1} = Y_{CO_2}/M_{CO_2} + Y_{CO}/M_{CO}, \quad (12)$$

$$Y_{c_2} = Y_{CO_2}/M_{CO_2} + Y_{CO}/M_{CO} + Y_{H_2O}/M_{H_2O} + Y_{H_2}/M_{H_2}. \quad (13)$$

This sort of definition is widely applied, and it has been used in recent works⁴⁶ with similar setups as the present study. Despite the apparent usefulness of (12) and (13), some shortcomings should be commented. The current work addresses the combustion of methane–oxygen at high pressures. In such a regime, the adiabatic flame temperatures can be remarkably high, leading to a significant contribution of ionization processes with the proliferation of free radicals.⁴⁷ These phenomena have direct consequences in terms of the relevant species presence. The mass concentration of hydroxyl Y_{OH} can be considerably high toward the reactants (over 10%).⁴⁸ The mass fractions of oxygen and hydrogen radicals can be significant as well. In addition, the hydrogen mass concentration Y_{H_2} peaks at mid-flame positions, and it drops before combustion ends.⁴⁸ Due to this non-monotonic behavior, Y_{H_2} is an ambiguous indicator. To correct these issues, it is more convenient to remove the contribution of hydrogen and replace it with products representative of high-temperature combustion. Hence, we propose the following expression for the reaction progress:

$$Y_{c_3} = Y_{CO_2}/M_{CO_2} + Y_{CO}/M_{CO} + Y_{H_2O}/M_{H_2O} + Y_O/M_O + Y_H/M_H + Y_{OH}/M_{OH}. \quad (14)$$

2. Length and time scales

Diffusion flames are characterized by two principal length scales:⁴⁹

- (a) The reaction zone thickness, which is marked here as δ_c , and it corresponds to the space where chemical reactions take place.
- (b) The diffusion layer thickness, denoted in this text as δ_D , and it is the extent of the region where the mixture fraction Z varies.

In the present work, δ_D and δ_c have been calculated considering averaged local gradients of the mixture fraction and the progress variable, respectively. The detailed procedure is described in the text below. In the laminar flame theory, the simplest procedure to determine the chemical length scale is to calculate the laminar flame thickness assuming linearity in the progress variable as follows:

$$\delta_L = \frac{1}{\max\{|\nabla c|\}}, \quad (15)$$

This result provides a lower bound for the flame front thickness since c gradients are smaller toward the extremes. The linear assumption works reasonably well in the case of methane at mid-flame positions, where the gradient of c is nearly constant.⁵⁰ Hence, one simple way to

assess the local flame thickness for intermediate values of c is as follows:

$$\delta_c(\bar{x}) = \frac{1}{|\nabla c(\bar{x})|}. \quad (16)$$

This definition provides accurate estimation for intermediate values of c , i.e., $0.3 < c < 0.7$. Using a DNS database, it is possible to determine an average chemical length scale $\bar{\delta}_c$ at a given position \bar{x} . Despite its physically meaningful definition, the provided expression for $\bar{\delta}_c$ poses major challenges due to its complex determination outside the realm of scale-resolving simulations. This circumstance significantly hinders this parameter's applicability. If the standard deviation of $|\nabla c|$ is small compared to its mean value, it is possible to approximate the average flame thickness as the inverse of the flame surface density Σ as follows:

$$\bar{\delta}_c \approx \Sigma^{-1} = 1/|\overline{\nabla c}|. \quad (17)$$

This approximation holds with an error below 20% throughout most of the shear layer in the performed simulations. Unlike $\bar{\delta}_c$, the transport of the flame surface density has already been approached,^{51–53} and existing models are available.

The diffusion thickness can be estimated using a similar procedure, resorting to the mixture fraction gradient as follows:

$$\delta_D(\bar{x}, t) \approx \frac{1}{|\nabla Z(\bar{x}, t)|}. \quad (18)$$

To prevent the non-linear effects, the use of this expression should be restricted to values close to stoichiometric conditions. Hence, the average diffusion thickness at a given position \bar{x} can be estimated as follows:

$$-\delta_D(\bar{x}) = -\frac{1}{|\nabla Z(\bar{x}, t)|_{Z=Z_{st}}} \approx \sqrt{\frac{2D_{st}}{\tilde{\chi}_{st}}}, \quad (19)$$

where D_{st} and $\tilde{\chi}_{st} = 2(\rho D |\nabla Z|^2|_{Z=Z_{st}})/\bar{\rho}$ stand for the mass diffusivity and the scalar dissipation rate at stoichiometric conditions. Within the present work, the approximation in (19) holds with an error below 5% throughout most of the shear layer and can therefore be regarded as accurate. The scalar dissipation rate is a central concept in non-premixed turbulent combustion, which requires further discussion. This parameter represents the mixing intensity and estimates the decay of mixture fraction fluctuations, playing a similar role as $\tilde{\epsilon}$ for the turbulent kinetic energy. From this notion, it is possible to define a characteristic timescale for the fluctuations around the mean mixture fraction $t_Z = \overline{Z'^2}/\tilde{\chi}$, which is often modeled to be proportional to the turbulent timescale t_T ,

$$t_T = \frac{\tilde{k}}{\tilde{\epsilon}} \approx c_\chi \frac{\overline{Z'^2}}{\tilde{\chi}}, \quad (20)$$

where c_χ is a model constant that varies from 1.5 to 3.⁴³ A value $c_\chi = 2$ is often used.⁴³ The model in (20) presents several deficiencies, as discussed in Sec. IV. The value $\tilde{\chi}$ alone is not necessarily entirely related to the combustion process. Hence, its conditional average at stoichiometric conditions $\tilde{\chi}_{st}$ is often more interesting to measure flame properties. The offset between $\tilde{\chi}_{st}$ and $\tilde{\chi}$ can be used to quantify

how likely is. Hence, low ratios $\tilde{\chi}/\tilde{\chi}_{st}$ denote that high above-average mixing is required for stoichiometric conditions to occur.

Using asymptotic theories,⁵⁴ the flame Damköhler number can be obtained by considering the introduced length scales as follows:

$$Da_{\beta l} = \frac{t_D}{t_c} \approx \left(\frac{\bar{\delta}_D}{\delta_c}\right)^a \approx \left(\frac{2D_{st}}{\tilde{\chi}_{st}\Sigma^2}\right)^{\frac{a}{2}}, \quad (21)$$

where a is a parameter dependent on the global chemical mechanism. For the case of methane–oxygen combustion, this exponent can be approximated as $a \approx 2$. The flame Damköhler number provides valuable information regarding the flame's structure stability^{49,55,56} and can be used to classify the regimes in non-premixed combustion.⁵⁶ In addition to these implications, the flame Damköhler number is relevant due to its relationship with the turbulent Damköhler number, which can be expressed as follows:

$$Da_T = \frac{t_T}{t_c} = \frac{t_T t_D}{t_c t_D} = \frac{t_T}{t_D} Da_{\beta l}. \quad (22)$$

If the diffusion thickness can be assumed to be controlled by the smallest vortical structures and it is possible to set $t_D \approx t_\eta$, yielding $Da_T \approx \sqrt{Re_T} Da_{\beta l}$.⁴⁹ This is not the case in the current work since the Kolmogorov eddies are expected to be significantly smaller than the chemical length scales. To approach this problem, it is necessary to find a suitable expression for the proportionality factor between both Damköhler numbers, which corresponds to the ratio between vortical timescales and diffusion timescales, i.e., t_T/t_D . The diffusion timescale can be expressed as the inverse of the Favre-averaged stoichiometric scalar dissipation rate, i.e., $t_D = 1/\tilde{\chi}_{st}$.⁴⁹ Hence, it is possible to recast the proportionality factor between Damköhler numbers as follows:⁴⁹

$$\frac{t_T}{t_D} = \frac{\tilde{k}}{\tilde{\epsilon}} \tilde{\chi}_{st}. \quad (23)$$

Inserting this expression in (22) yields

$$Da_T = \frac{\tilde{k}}{\tilde{\epsilon}} \tilde{\chi}_{st} Da_{\beta l}. \quad (24)$$

One relevant aspect involving this definition is its conditionality to stoichiometric conditions. Because of this particularity, this Damköhler number is representative of the instants when a stabilized diffusion flame is present. Therefore, this definition is able to capture the mixing enhancement due to the flame's thermal expansion but neglects quenching events. Substituting $\tilde{\chi}_{st}$ by $\tilde{\chi}$ in (24) provides a value denoted in this text as Da_T^* , which is related to the complete flow statistics at a given position. This value shall be more suitable for modeling the integral interactions between the flame's turbulence and combustion.

III. SIMULATION SETUP

This section is devoted to the simulation setup description. The text is structured in two main parts. First, the overall simulation strategy is discussed, including a brief description of the turbulence and chemistry characteristics. Second, the primary resolution requirements associated with DNS in turbulent combustion are discussed, and their degree of achievement in the current work is studied.

A. Simulation strategy

A standing non-premixed flame was simulated in a cuboid domain with an aspect ratio of 5 using DNS. Periodicity is imposed in two directions (xy), perpendicular to the main flame’s propagation direction (z). The performed computations can be divided into two main segments. First, the unmixed flow develops into physically meaningful turbulence in a precursor simulation. The resulting velocity fields are subsequently used to feed the turbulent inlet of the main simulation. This setup is represented in Fig. 1. The main simulation’s domain comprises a cuboid volume with dimensions $0.2 \times 0.2 \times 1 \text{ mm}^3$, resolved with $144 \times 144 \times 720$ uniform cubic cells. Oxygen and methane are injected at the inlet with contiguous equal areas. This sort of arrangement implies a region with an unusually steep concentration gradient. It is not clear if the results observed in this part are relevant to actual diffusion flames. In an actual combustor, a non-slip wall separates the oxidizer and fuel injection, creating a recirculation zone and preventing the high concentration gradients that appear in the simulation performed for the current study. Investigating this region’s fluid dynamics poses a formidable challenge, which exceeds the present text’s scope. The results in this zone will be displayed for the sake of completeness, but they should be taken with care. As one moves downstream, the flow shortly recovers from the steep inlet boundary condition. After roughly ten times the laminar flame thickness $z \approx 10\delta_{L0}$, the flow resembles a canonical reactive shear layer, and the simulation’s results are entirely relevant. Zero gradient boundary condition is applied at the domain’s outlet for every field.

Since velocity fluctuations are very small compared with mean velocities in this region, backflows are not expected, ensuring the stability of the chosen boundary condition.

Although the domain is three-dimensional, its statistics can be significantly simplified. Since the boundary conditions are independent of the Y -direction, it can be assumed that the turbulence statistics are invariant in this direction. The symmetry of statistical properties can be assumed following similar reasoning. Hence, the simulation results are averaged in time, y , and symmetry. This is the default procedure for calculating all the presented statistical results in the following unless otherwise stated.

In the precursor simulation, periodic synthetic turbulence is generated with the scheme described in Ref. 57, based on the strategy devised by Shur *et al.*⁵⁸ This method is based on the superposition of randomized harmonics following a reference spectrum as originally proposed by Kraichnan.⁵⁹ The synthetically generated velocity field develops with enough length to ensure convergence into a mature turbulent flow. Species concentrations are enforced during this development to disable mixing. The turbulent properties were chosen to resemble the results obtained at RANS simulations for a scale methane rocket combustor described in previous works.⁶⁰ The mass diffusion coefficients are set to zero in this segment to disable mixing. Due to the different physical properties, the developed turbulent characteristics of the methane and fuel sides are slightly different after convergence. The plane where oxygen and methane meet constitutes a shear

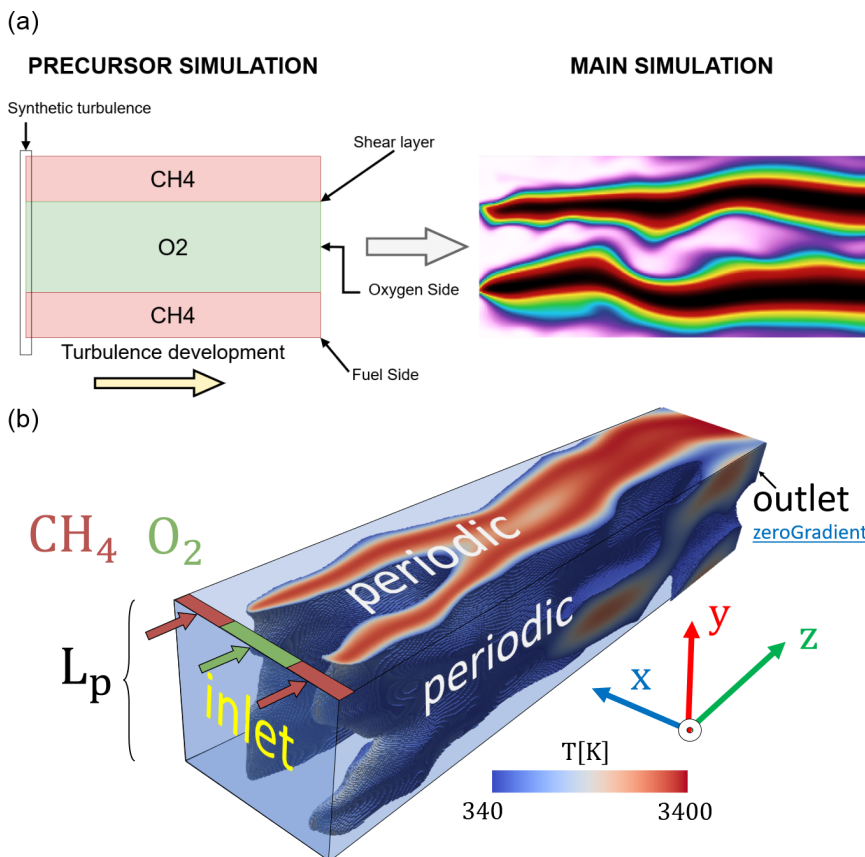


FIG. 1. Overview of the simulation strategy: simulation sequence (a), schematic of the main simulation domain and boundary conditions (b); cells with temperatures below 340 are filtered out to maximize the observability of the flame’s 3D structure.

16 April 2024 08:28:26

layer whose turbulent properties require commenting. The dissipation rate of turbulent kinetic energy is remarkably enhanced in this region due to the steep gradients in density and velocity. This effect leads to a higher concentration of vorticity with lower eddy lifetime and length scales. The most relevant turbulent characteristics were evaluated at the end of the precursor segment at each relevant position, and the results are displayed in Table I. The points where these parameters were evaluated correspond to the ones signaled in Fig. 1(a). The developed turbulent field presents similar characteristics at the fuel and oxidizer sides. Nevertheless, the oxygen part exhibits slightly higher turbulence levels due to its lower kinematic viscosity. The consequences of the enhanced dissipation rate at the shear layer can be observed in the last column in Table I. The relevant Reynolds numbers in this surface are remarkably lower due to the smaller size of the largest eddies, which originated from the breakup of larger vortical structures. This turbulent intensity remains within the order of magnitude of the targeted study application, although higher Reynolds numbers would be desirable to reproduce more representative scenarios. Such conditions were not implemented due to the high associated computational cost.

The main simulations were conducted with the reactive solver EBI (Engler-Bunte-Institut) — DNS,^{61–64} based on the open-source software OpenFOAM,^{65,66} which solves the conservation equations for mass, momentum, energy, and species in compressible flows using the finite volume method (FVM).^{67,68} This solver has been applied and validated over a wide variety of combustion-related problems.^{69–73} Detailed chemistry and transport properties are computed with Cantera,⁷⁴ using the mixture-averaged transport model as described by Kee *et al.*⁷⁵ The skeletal mechanism developed by Slavinskaya *et al.*⁷⁶ is used to compute methane combustion using finite rate. This reaction mechanism consists of 21 species and 97 reactions, and it is conceived for space propulsion applications at high pressures. The relevant combustion parameters are summarized in Table II. The injection velocity s_i is chosen to be small enough to avoid flame quenching and high enough to allow the development of an observable reactive shear layer. This velocity is the same for both oxygen and methane to ensure that mixing processes are entirely driven by turbulence, filtering out the shear effect.

B. Resolution requirements

Direct numerical simulations come at the highest cost since they require resolving all the relevant fluid and chemical processes scales.

TABLE I. Relevant turbulent scales and characteristics in the different unburnt regions. Physical quantities are normalized with the laminar flame characteristics at stoichiometric conditions, i.e., δ_{L0} and s_{L0} , which can be consulted in Table II.

	Fuel side	Oxidizer side	Shear layer
η/δ_{L0}	0.175	0.175	0.2
λ/δ_{L0}	1.99	2.1	1.72
Λ/δ_{L0}	4.3	5.31	2.06
L/δ_{L0}	7.9	9.77	3.78
u'/s_{L0}	1.15	1.13	1.06
Re_λ	32.4	38	18
Re_T	69.9	96.2	21.62
Re_L	128.5	176.7	39.72

TABLE II. Main combustion parameters of the simulated flame.

P	Pressure	20 bar
T_u	Temperature of the unburnt reactants	300 K
ϕ	Global equivalence ratio	0.5
δ_{L0}	Laminar flame thickness at stoichiometric conditions	5.505 μm
s_{L0}	Laminar flame speed at stoichiometric conditions	2.5735 m/s
s_i/s_{L0}	Normalized bulk velocity of the unburnt gases	2.72
s_b/s_{L0}	Normalized velocity of the combustion products	21.51

From the standpoint of fluid mechanics, resolution requirements are driven by the Kolmogorov scale and the integral size of the eddies. More specifically, it is recommended to resolve the Kolmogorov eddies with 1/2.1 cells²² and to make a domain large enough so that it can contain at least eight eddies with the integral size Λ .²¹ These requirements can be formalized with the following performance indicators:

$$r_\eta = 2.1\bar{\eta}/\Delta x, \quad (25)$$

$$r_\Lambda = L_p/8\bar{\Lambda}. \quad (26)$$

These parameters present a value greater than unity if the requirement is fulfilled.

The flame front resolution constitutes the main requirement from the standpoint of chemistry. In the context of premixed flames, 10 to 20 cells per laminar thermal flame front thickness are usually recommended.⁷⁷ However, diffusion flames cannot be characterized with a single length scale as previously discussed. To circumvent the spatial variability, it is reasonable to consider the local reaction thickness defined in (16) as reference parameter for the zonal chemical length scale. Taking the lower bound of ten cells, it is possible to express the normalized chemistry resolution achievement as follows:

$$r_c = 0.1\bar{\delta}_c/\Delta x. \quad (27)$$

The degree of achievement of the three mentioned resolution requirements is summarized in Fig. 2. This illustration represents the cumulative distribution function of the normalized resolution accomplishment. The only indicators that are not being fulfilled at every cell are the

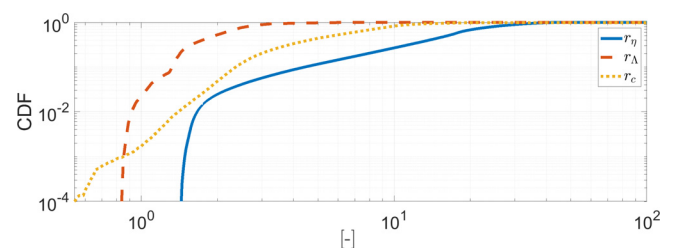


FIG. 2. Cumulative distribution function of the different resolution requirements degree of achievement. Values are normalized so that lower than unity implies unfulfillment and greater than one implies fulfillment.

periodicity length and flame front resolution. The flame front is resolved with less than ten cells at approximately 0.1% of the positions. The domain is not large enough to contain eight integral eddies for approximately 2% of the cells. Hence, the regions at which resolution requirements are not attained represent a low fraction of the simulated volume. Furthermore, the resolution at these locations is close to the target values (over 90%). In addition, most of the cells lacking completeness in resolution requirements are placed at the near injection region (NIR), which is of limited interest within the present work's scope. Overall, it can be concluded that the simulation setup fulfills the spatial DNS requirements well enough to ensure high fidelity in the observed statistics.

Regarding the necessary simulation time, it is necessary to reproduce the temporal evolution of enough vortical structures to achieve an ergodic dataset. This is usually evaluated in terms of a reference eddy turnover time. The properties of the unburnt oxygen side have been taken as a reference since it presents the largest vortical timescales, constituting the worst-case scenario. The present simulation has been run for 32 times this reference eddy-turnover time. Field data for density, pressure, temperature, velocity, and species were collected with a frequency of roughly 18 times per eddy turnover time. The time step size is adaptive, ensuring maximum local CFL (Courant–Friedrichs–Levy) number below 0.4. An example of instantaneous results is displayed in Fig. 3. This graph presents obtained solution and the normalized second invariant $Q = (\|\Omega_{ij}\|^2 - \|S_{ij}\|^2)^{78}$, with $\Omega_{ij} = \frac{1}{2} \left(\frac{\partial u_i}{\partial x_j} - \frac{\partial u_j}{\partial x_i} \right)$, and $S_{ij} = \frac{1}{2} \left(\frac{\partial u_i}{\partial x_j} + \frac{\partial u_j}{\partial x_i} \right)$ representing enstrophy and shear stress rate. The fields for oxygen and rho provide valuable information regarding the flame's development and $Q/\|\Omega_{ij}\|^2$ can be taken as an indicator of the vortex presence.

Thanks to the symmetry of the turbulence statistics, twice the amount of information can be obtained from each time step. In practical terms, this implies that the amount of available data effectively

adds up to 78 eddy turnover times. Such a number of observations is large enough to ensure high confidence in the obtained statistics.

IV. RESULTS

This section is devoted to the discussion of the simulation outputs. The text is structured in two main parts. First, the development of the diffusion flame is studied, and the relevant combustion parameters are presented. Second, the transport of turbulence is analyzed. Some previous remarks shall be stated to ease the understanding of the upcoming discussion. The reader will observe gaps at certain graphs where no results are plotted. These data holes originate from the lack of observations in conditional analyses. For example, when calculating the scalar dissipation at stoichiometric conditions, such a state may never take place at certain locations, precluding this parameter's calculation. During the result's discussion, the adjectives inner and outer will denote the oxygen- and fuel-rich regions, respectively. In addition, the terminology radial and axial will be used to denote directions x and z , respectively. This nomenclature is used since it is easy to relate to the presented graphs and with actual coaxial injectors. Nevertheless, it is important to remark that this terminology is not entirely accurate from a physical standpoint.

A. Flame characteristics and development

The Favre-averaged mixture fraction and progress variable is presented in Fig. 4. The simulated flame's structure resembles that of triple flames.^{79,80} In particular, the non-premixed flame is located nearby the region where $\tilde{Z} \approx Z_{st} \approx 0.2$, with the lean and rich premixed branches placed at $\tilde{Z} < Z_{st}$ and $\tilde{Z} > Z_{st}$, respectively. Due to the symmetric configuration, two triple points placed at $z = 0$ and $x \approx \pm 10\delta_{L0}$ are present. The progress of the reactive shear layer can be observed until the position $z \approx 60\delta_{L0}$. Before this point, two shear layers are present, each of them characterized with a fuel-rich and an oxygen-rich side.

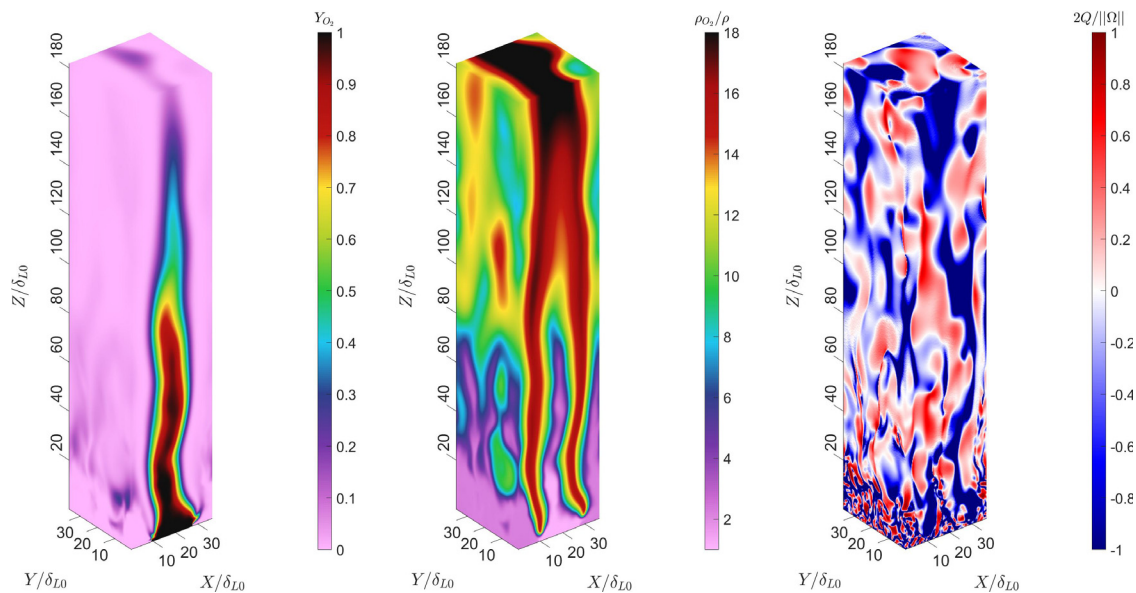


FIG. 3. Example of instantaneous field results: oxygen concentration Y_{O_2} (top left), hydroxyl concentration Y_{OH} (top right), normalized specific volume ρ^{-1} (bottom left), and normalized second invariant Q (bottom-right).

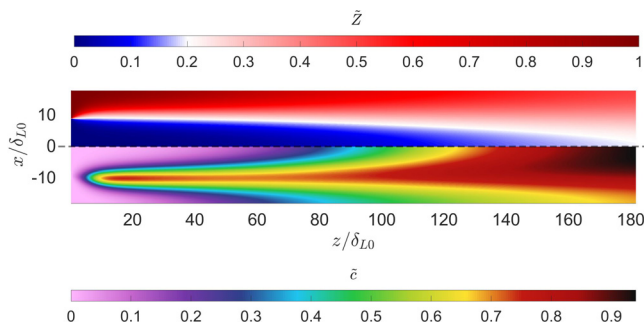


FIG. 4. Favre-averaged mixture fraction and progress variable.

Afterward, both layers merge into a single structure. The collision between the shear layer occurs at the oxygen-rich side. This fact is motivated by the higher agility of methane-related molecules, which can reach the inner region before their oxygen counterparts arrive on the fuel-rich side. Consequently, the chemical reactions following the shear layer merging are restricted to the interface between the fuel-rich side and the inner region. These remarkable differences in chemical processes significantly influence the transport of turbulent properties, which are discussed in more detail in Sec. IV B. Close to injection, at roughly $z \approx 20 \delta_{L0}$ a local maximum of the averaged progress variable can be observed. This result is, in principle, counterintuitive since a gradual increase in the progress variable in the axial direction shall be expected. The region where this peak takes place coincides with a local maximum of $\tilde{\chi}/\tilde{\chi}_{st}$, which indicates that small mixing intensity is required to achieve stoichiometric conditions. Hence, the presence of the local maximum of $\tilde{\chi}/\tilde{\chi}_{st}$ denotes a trend to shift away from stoichiometric conditions as the flow moves axially.

We hypothesize that these processes are motivated by the sudden slow-down of chemical speed, illustrated by the different Damköhler numbers in Fig. 5. The combustion in the near injection region (NIR) is entirely driven by small-scale turbulence, which favors the fast

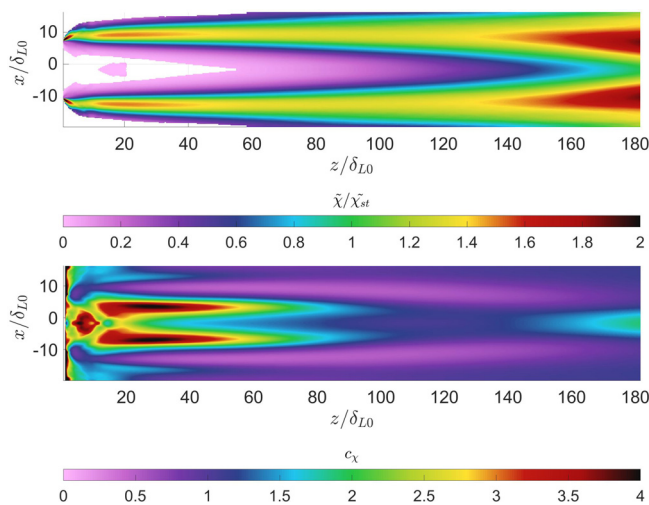


FIG. 5. Estimated Damköhler numbers at the simulation's domain. Top: flame Damköhler number. Bottom: turbulent Damköhler number.

consumption of all available reactants nearby the mean reactive shear layer. By $z \approx 20 \delta_{L0}$, reactants are depleted at the center of the reactive shear layer with the subsequent drop of the turbulent Damköhler number Da_T . This steep variation is caused by the sudden unavailability of fresh reactants coupled with the fact that eddies have not yet experienced significant accumulated decay. In such a context, material advection is the dominating effect in species transport. This condition explains the moderate decrease in the progress variable as the flame advances axially. The fuel- and oxygen-rich sides of the shear layer eventually experience a similar evolution, consuming the immediately available reactants with the subsequent decrease in the Damköhler number. By $z \approx 70 \delta_{L0}$, the Damköhler number becomes homogeneously small through the shear layer. From this position, the large-scale diffusion processes become the driving factor in the reactive shear layer development and a consistent increase in the progress variable in axial direction can be observed.

Another relevant output from the performed simulations is the proportionality factor c_χ between eddy length scales and fluctuations in the mixture fraction, which can be observed at the bottom of Fig. 6. The observed values are close to the expected ones. Nevertheless, some relevant discrepancies shall be addressed. First, the “constant” c_χ presents a variable behavior through the flame's domain, which indicates that additional phenomena cannot be captured with this simple model. Second, there is a significant variation between the fuel-rich and the lean sides. We hypothesize that these variations are driven by the intermittent behavior of the flame in the oxygen-rich region, driven by flammability constraints. Due to the limited mobility of oxygen molecules, the outer region's reactive behavior is limited by the oxidizer's advection in radial direction. This effect, coupled with the asymmetry in the flammability limits, precludes the constant presence of a stable flame on the lean side. In the absence of combustion, mixture fraction fluctuations are solely driven by mass diffusion processes, filtering out the flame's self-diffusion enhancement caused by thermal

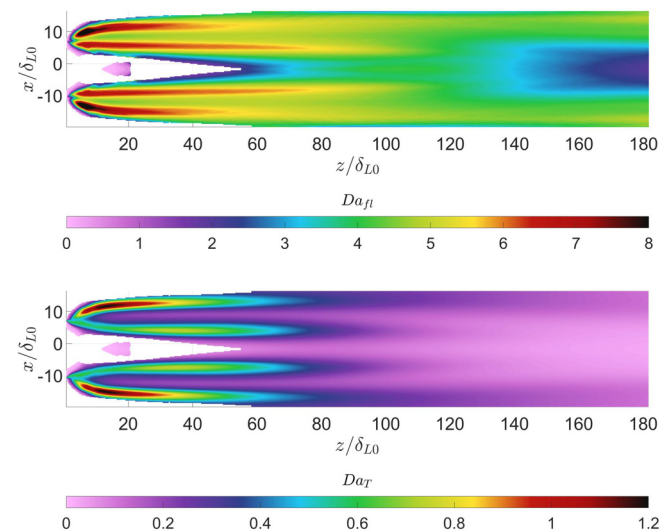


FIG. 6. Scalar dissipation rate graphs. Top: ratio between scalar dissipation rate and scalar dissipation rate at stoichiometric conditions. Bottom: model constant c_χ relating vortical timescales to timescales in terms of mixing ratio fluctuations.

expansions. Indeed, if the timescales of mixture fraction fluctuations are conditionally averaged to stoichiometric conditions, a consistent value through all the shear layer is obtained.

The turbulent Damköhler number was calculated both at stoichiometric and general conditions. Regardless of the approach, the Damköhler remains constant within the central region of the shear layer. Nevertheless, remarkable differences can be observed in the shear layer’s lean periphery. When only stoichiometric conditions are considered, turbulent and chemical timescales appear to be in the same order of magnitude. However, when properties are not conditionally averaged, vortical structures outspeed the mean chemical timescales. This behavior is motivated by the lower flame consistency in the lean region, which was described previously.

B. Turbulence transport

The Favre-averaged turbulent kinetic energy and its dissipation rate are represented in Fig. 7. Generation of turbulent kinetic energy can be observed at specific locations of the mean flame. The first spot of turbulence generation appears at the NIR, and it is associated with high values of dissipation rate as well. This result is caused by the steep gradients in species concentration, which generate abrupt dynamics with short timescales. The turbulent kinetic energy decreases shortly downstream, and it reaches a local minimum at roughly the same position where the local maximum of \tilde{c} was observed. In addition, turbulence is generated at the shear layer’s periphery, coinciding with the progress variable progression. This evidence a combustion-driven turbulence generation, which is commented. After the shear layers merge, a rather constant spatial decay can be observed, leading to a monotonically decrease in turbulent kinetic energy. This behavior corresponds to the second half of the simulation volume, where chemical reactions are marginal, and the progress variable almost behaves like a passive scalar. Hence, the coupling between chemistry and turbulence is weakened, and viscous dissipation becomes the dominating mechanism of turbulent transport.

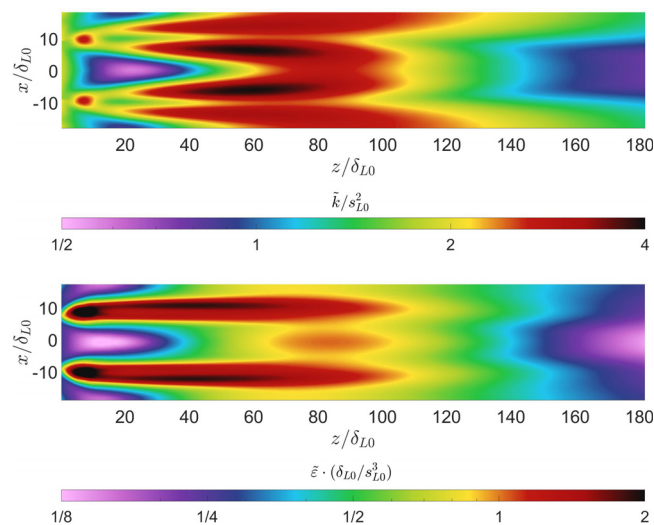


FIG. 7. Normalized Favre-averaged turbulent kinetic energy and its dissipation rate.

The turbulent kinetic energy transport budget was studied in detail to investigate the mechanisms responsible for the afore-described behavior. The global turbulent transport is presented in Fig. 8, and it is decomposed in its individual terms in Fig. 9. Turbulent transport through mean pressure gradients (i.e., T_2) is the main source of turbulent kinetic energy together with the other two pressure terms (i.e., T_3 and T_5). These terms are able to counter the dissipative term (T_4) in the first region of the flame. This overall result is very similar to what has been observed in flames operating in the corrugated flamelet regime.^{9,23} Nevertheless, relevant radial variations, which do not take place in a statistically planar premixed flame, can be observed as well. These differences are commented on in detail in the following Secs. IV.B.1–IV.B.5.

1. Turbulence production through mean velocity gradients T_1

The turbulent production term T_1 is usually negative in the context of a statistically planar turbulent deflagration.^{9,10,23,24,29} Negative values for T_1 have also been reported in jet flames with low turbulent intensity due to misalignments between the principal directions of the Reynolds stress tensor (RST) and the flame normal direction.⁸¹ It is important to remark that this is not the case within the flame studied in the present paper as the principal directions of the local RST are almost perfectly aligned with the mean flame propagation direction at almost every position. Therefore, the preponderance of negative values for T_1 originates from the flow’s acceleration in the flame’s normal direction. In addition to the predominance of negative production displayed in Fig. 9, positive values at certain regions near to injection can be observed. To understand this behavior, it is necessary to discuss the evolution of velocity gradients in all directions. The mean axial velocity has a positive gradient everywhere, causing negative values of T_1 for most of the domain. The higher magnitude of these gradients occurs at regions with good mixing due to the promotion of chemically induced thermal expansions. In areas where the local mixture fraction is outside the flammability limits, combustion cannot occur, and the axial velocity gradient is small. This case corresponds to the zones within the diffusive shear layer but outside the reactive shear layer, where the mixture fraction tends to unity. In these cases, mass diffusion and advection of reactants produces radial velocity gradients, while axial velocity gradients are small since the chemistry is marginal with $Da_{fl} \approx 0$. In other words, mixing in the absence of combustion takes place. Since thermal expansion is not the main driver of mean velocity gradients, positive values for T_1 become viable at these locations.

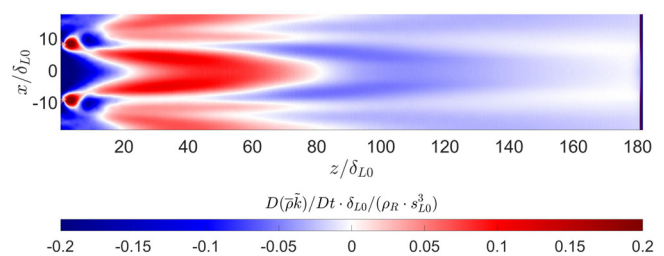


FIG. 8. Normalized global turbulent transport through the simulated diffusion flame.

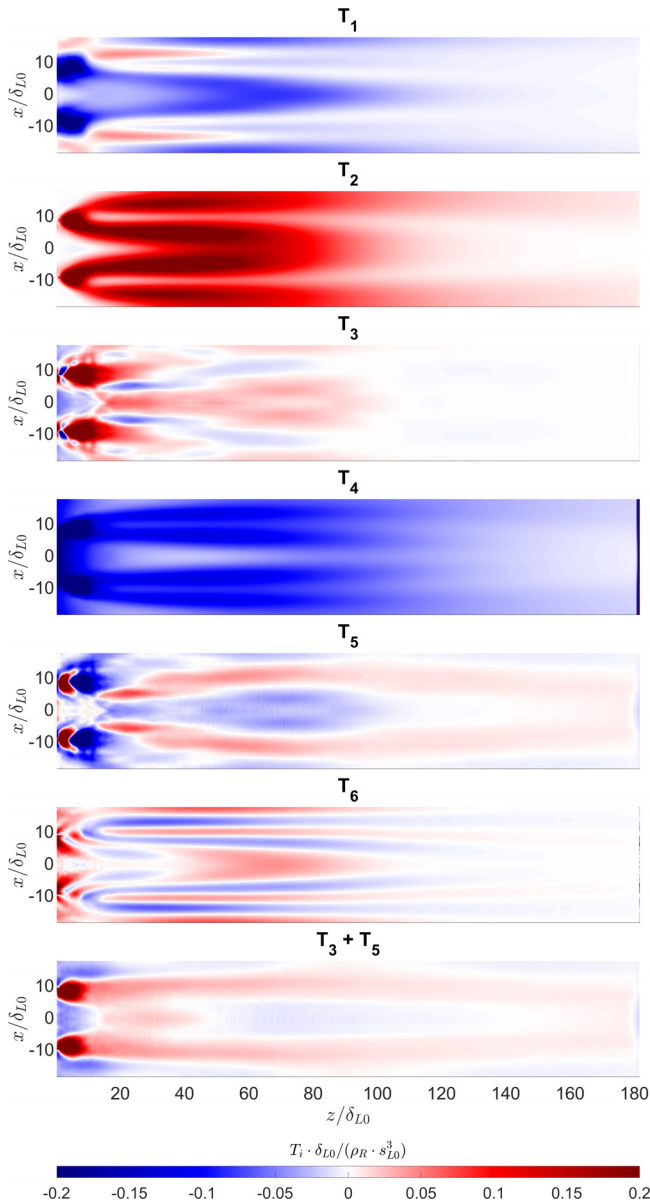


FIG. 9. Turbulent transport budget through the simulated diffusion flames.

2. Turbulence production through mean pressure gradients T_2

In the frame of RANS, $\partial \bar{p} / \partial x_i$ is closed, and hence modeling T_2 only requires closing the averaged Favre velocity fluctuations, i.e., $\overline{u_i''}$. For premixed flames, Nishiki *et al.*²⁴ proposed the following model:

$$\overline{u_z''} = \frac{\tau_\alpha}{\rho_0} \overline{\rho u_z'' c''}. \quad (28)$$

This expression provides excellent agreement with observations in DNS of premixed flames.^{9,24,29} Nevertheless, some aspects should be addressed. The derivation proposed by Nishiki *et al.* is based on a local

thin flame front assumption and linearizations, being valid for small density ratios $\sigma = \rho_R / \rho_P$. In flames where air is used as oxidizer, $\sigma < 5$; this assumption can be rendered as valid. Nevertheless, in the context of rocket engines combustion, the density ratio can easily rise above 10. Another core requisite in the derivation of (28) is that c and ρ are linearly correlated. This assumption is valid for premixed flames, where variations in density are mainly associated with combustion development. However, in non-premixed flames, mixing drives additional density variation processes in the absence of combustion, effectively decorrelating c and ρ . Hence, it is first necessary to assess the viability of Nishiki model for closing T_2 in non-premixed combustion. It is possible to adapt the original formulation by Nishiki *et al.* for non-premixed combustion as follows:

$$\overline{u_z''} = f_\tau \frac{-\tau_{z0}}{\rho_{fu,0} + (\rho_{ox,0} - \rho_{fu,0})\tilde{Z}} \overline{\rho u_z'' c''}, \quad (29)$$

where f_τ is a correction coefficient, taking into account the fact that the effective heat release parameter is below the one at stoichiometric conditions, i.e., τ_{z0} . This adapted formulation was tested for the data obtained in the performed simulations. The result is presented in Fig. 10. A value $f_\tau \approx 0.84$ was found to maximize the fitting with the simulation's output. As it can be seen, the agreement is excellent through the shear layer and in the NIR. Hence, it is reasonable to use (29) as a baseline for achieving closure of T_2 .

The following required step is modeling the turbulent scalar flux $\overline{\rho u_z'' c''}$. Traditionally, gradient transport assumptions have been used to approach this sort of terms in turbulent combustion models.^{82–84} Nevertheless, the use of this methodology for modeling $\overline{\rho u_z'' c''}$ has revealed extremely poor within the present work. The results are not reproduced in this text for the sake of conciseness. In premixed flames, it is possible to resort to the BML approach²⁵ to obtain the following expression for the required scalar flux:

$$\overline{\rho u_z'' c''} \approx \bar{\rho} \tilde{c} (1 - \tilde{c}) (\overline{u_{zP}} - \overline{u_{zR}}), \quad (30)$$

where $\overline{u_{zP}}$ and $\overline{u_{zR}}$ denote the mean, i.e., bulk velocity of the products and the reactants, respectively. This expression can be used as a departure point to build an analog formulation for non-premixed flames. In particular, the following expression can be considered:

$$\overline{u_z''} = s_{L0} C_2 \bar{\rho} C_{cZ} f_{cZ}(\tilde{c}, \tilde{Z}), \quad (31)$$

where C_2 is a model constant, $f_{cZ}(\tilde{c}, \tilde{Z})$ is a shape-form function with the form $f_{cZ}(\tilde{c}, \tilde{Z}) = \tilde{c}^{n_c} (1 - \tilde{c})^{m_c} \tilde{Z}^{n_z} (1 - \tilde{Z})^{m_z}$, and C_{cZ} is a coefficient such that $\int_0^1 \int_0^1 f_{cZ}(\tilde{c}, \tilde{Z}) d\tilde{c} d\tilde{Z} = 1/36$. The function f_{cZ} performs

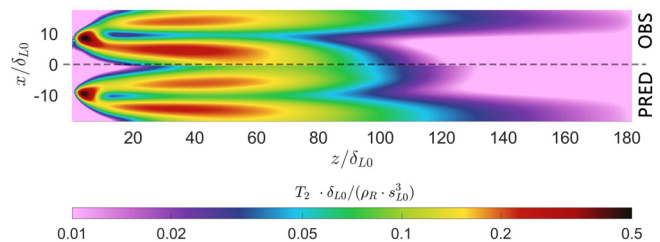


FIG. 10. Observed and predicted values for the turbulence production by mean pressure gradients T_2 using the unclosed Nishiki model.

an analog role as the expression $\tilde{c}(1 - \tilde{c})$, with the coefficients n_c and m_c , enabling skewed shape, which is a common result in non-premixed combustion statistics. The effect of variable mixture fraction is captured with the same sort of expression. The proposed model has in total five degrees of freedom (n_c, m_c, n_Z, m_Z, C_2). The values of these coefficients were optimized to maximize the fitting with the current simulation's output. The model's performance can be observed in Fig. 11. As it can be seen, the agreement is rather good both qualitatively and quantitatively through most of the domain. Nevertheless, the model's prediction in the NIR is rather deficient, which is likely to be related to the complex dynamics in this region.

The performance of the discussed models is illustrated in Fig. 12. The data was axially averaged in this graph to simplify the comparison between the different models as combustion evolves. As it can be seen, Nishiki's model remains very close to the observed data, especially downstream, where the flow conditions are almost premixed. The proposed closed model overpredicts turbulence generation at the NIR and downstream, and it underpredicts turbulence transport at the reactive shear layer. The main reason for the latter mismatch is the model's failing in the anticipation of high turbulence generation at premixed branches of the triple flame. Overall, the proposed closed model exhibits a worse performance compared to the adapted version of Nishiki's model. This result is in principle expected, since it lacks access to the turbulent scalar flux $\rho u_z'' c''$.

3. Fluctuating pressure terms $T_3 + T_5$

As mentioned in Sec. II, it is more convenient to study the terms T_3 and T_5 in an aggregated way since the resulting mathematical expression simplifies the object of study. An original formulation was proposed by Launder *et al.*³⁵ for non-reacting flows. Zhang and Rutland²³ conceived an alternative approach for premixed turbulent flames. These two models can be combined, leading to the following expression:

$$T_3 + T_5 = \underbrace{C_{35,\Sigma} \Sigma s_{L0}^3 \rho_R \tilde{c}(1 - \tilde{c})}_{T_\Sigma} + \underbrace{C_{35,\Pi} T_\Pi}_{T_\Pi} + \underbrace{C_{35,\epsilon} \overline{D\tilde{e}}}_{T_\epsilon}, \quad (32)$$

where $C_{35,\Sigma}$, $C_{35,\Pi}$, and $C_{35,\epsilon}$ are the model constants. The term T_Σ considered individually corresponds to the Zhang and Rutland model. This term was originally derived assuming very thin local flame fronts with pressure drops governed by the typical compressibility mechanisms in weak deflagration. Hence, T_Σ embeds information concerning the combustion process, presenting non-negative values. The terms T_Π and T_ϵ correspond to the model formulated by Launder

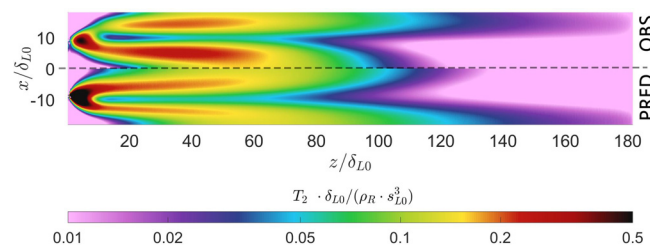


FIG. 11. Observed and predicted values for the turbulence production by mean pressure gradients T_2 using the closed method derived in this work.

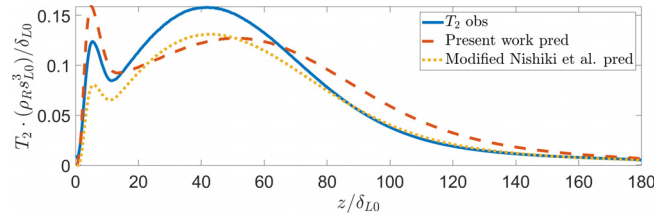


FIG. 12. Radially averaged turbulent kinetic energy transport through mean pressure gradients. The predicted value (blue continuous line) can be compared with the one resulting with the adaption of Nishiki's model to diffusion flames (red dashed line) and the proposed closed model (yellow dotted line).

*et al.*³⁵ and aim at predicting the behavior in the regions where combustion is marginal. Within the frame of non-premixed combustion, dissipative effects due to mixing should be considered in addition to the introduced terms. This factor can be incorporated by defining an additional term analogous to T_ϵ . Assuming that these effects scale with the scalar dissipation rate and the thermal diffusivity and adding reference parameters to achieve consistency in units, the following expression can be obtained:

$$T_\chi = C_{35,\chi} \frac{s_{L0}}{\delta_{L0}} \tilde{\chi} \tilde{\alpha} \bar{\rho}, \quad (33)$$

where $C_{35,\chi}$ is a model constant. Merging all the terms provides leads to the following model:

$$T_3 + T_5 = T_\Sigma + T_\Pi + T_\epsilon + T_\chi. \quad (34)$$

This model presents four degrees of freedom, which must be determined by resorting to observations. These defining constants were calculated to maximize the fitting with the performed simulations results. The predicted and observed values for $T_3 + T_5$ are displayed in Fig. 13. The limitations of this approach are quite evident. The model is able to capture some characteristics of the observed field, but the overall performance is very poor. Accurate prediction of the fluctuating pressure gradients has been traditionally complex to model in past research and remains as one of the main challenges to achieving closure in (7).

Despite the obvious limitations of the attempted modeling, some relevant insights can be extracted. The term T_χ , which is essentially negative is the best predictor in (34). Since the value of T_{FPG} varies from negative to positive, the primary deficiency lies in finding an appropriate source term. Overall, it can be concluded that closing

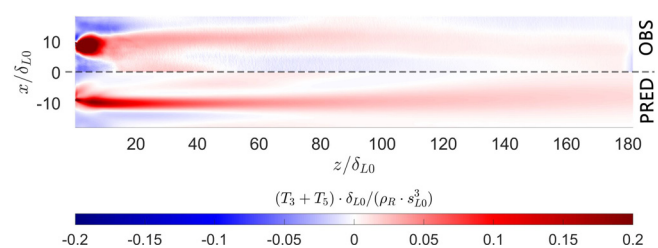


FIG. 13. Observed and predicted values for the pressure fluctuation gradients $T_3 + T_5$.

T_{FPG} in diffusion flames requires the incorporation of specific elements that have not yet been considered in the literature.

4. Dissipation term T_4

The term T_4 constitutes the principal turbulent kinetic energy sink in the context of premixed flames. In this sort of environment, the dissipation rate of turbulent kinetic energy represents the main contribution and the approximation $T_4 \approx -\bar{\rho}\bar{\epsilon}$ remains valid through all premixed flame regimes due to the low values of T_V and the molecular viscous transport $\nabla(\mu\nabla\tilde{k})$ in (9). To study the validity of this assumption, the offset of the expression $T_4 / -\bar{\rho}\bar{\epsilon}$ with respect to unity was calculated. The results are displayed in Fig. 14. As it can be observed, $T_4 \approx -\bar{\rho}\bar{\epsilon}$ does not hold through most of the domain. The dissipation of turbulent kinetic energy is enhanced at the extreme sides of the shear layer, whereas it is inhibited in the inner region. The reason behind this offset is the molecular viscous transport, which can be approximated as $\nabla(\mu\nabla\tilde{k}) \approx \partial(\mu(\partial\tilde{k}/\partial x))/\partial x$. This component presents large values due to the viscosity gradients perpendicular to the mean shear layer. Since this term is closed, this behavior does not pose a challenge from the standpoint of turbulence modeling. Although the term T_V is unclosed and technically requires modeling, it is of secondary importance. This value remains negligible through most of the domain and the approximation $T_4 \approx -\bar{\rho}\bar{\epsilon} - \partial(\mu(\partial\tilde{k}/\partial x))/\partial x$ holds almost perfectly through all points. More specifically, a relative error below 5% is found through most of the reactive shear layer, with discrepancies on the order of 10% at the NIR.

5. Turbulent transport through gradients of the turbulent flux of kinetic energy T_6

The term T_6 represents the gradient of the triple correlation of velocity fluctuations. In the shear layer of a diffusion flame, spatial derivatives of properties tend to be significantly larger in the direction perpendicular to the shear layer, compared with the mean flow's propagation direction. Within the current simulation frame, this claim implies that gradients in x are very large compared to gradients in z . The output of the performed simulations supports this assumption for the case of T_6 . Hence, it is possible to approximate this term as follows:

$$T_6 \approx \frac{-1}{2} \frac{\partial}{\partial x} \overline{\rho u_x'' u_k''^2} = \frac{-1}{2} \frac{\partial}{\partial x} \left(\overline{\rho u_x'' u_x''^2} + \overline{\rho u_x'' u_y''^2} + \overline{\rho u_x'' u_z''^2} \right). \quad (35)$$

This expression embodies the gradient of the correlation between the mass flux fluctuations perpendicular to the shear layer and “instantaneous” turbulent kinetic energy $u_k''^2$. Mass flux fluctuations induce the advection of vortices, whose turbulent kinetic energy scales

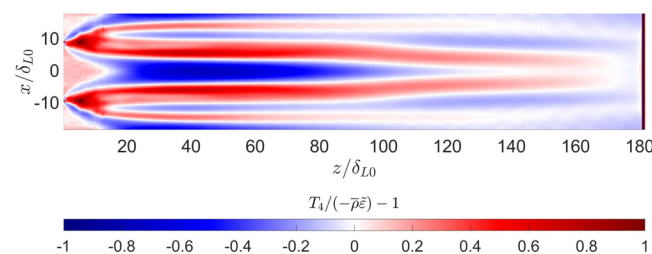


FIG. 14. Offset between T_4 and the dissipation rate.

with the gradient of \tilde{k} in the direction opposite to the incoming flux anomaly. This is the basis for the isotropic gradient model, which can be written for the present case as follows:

$$T_6 \approx \frac{-1}{2} \frac{\partial}{\partial x} \left(C_\mu \bar{\rho} \frac{k^2}{\epsilon} \frac{\partial k}{\partial x} \right), \quad (36)$$

where C_μ is a constant parameter approximated as 0.09 in the most extended models.²⁸ Daly and Harlow⁸⁵ proposed a generalized gradient model to cope with strongly non-isotropic flows. Departing from their formulation, the following expression can be derived:

$$T_6 \approx \frac{-1}{2} \frac{\partial}{\partial x} \left(C_s \bar{\rho} \frac{k}{\epsilon} \left(\overline{u_x'' u_x''} \frac{\partial k}{\partial x} + \overline{u_x'' u_z''} \frac{\partial k}{\partial z} \right) \right). \quad (37)$$

Both models were tested against the performed simulation's output. The results are presented in Fig. 15. The performance is overall good for both models. The anisotropic model is able to predict slightly better the turbulent transport in the lean region of the shear layer, but it exhibits a worse performance in the NIR. Both models overpredict the thickness of the shear layer's inner region where $T_6 > 0$ and underestimate the values in this area. However, the main inconsistency presented by both models appear in the lean region right after injection, where an inner region with $T_6 < 0$ is observed but none of the models foresees it. This region is meant to be challenging since it does not belong to a consistent shear layer and partial recirculation can occur.

Regarding the optimal parameters, the values 0.0766 for C_μ and 0.171 for C_s maximized the fitting of (36) and (37), respectively, which is in good agreement with the constants found in the literature. If the first section of the domain ($z < 40\delta_L$) is excluded from the optimization procedure, the optimal values result in 0.087 for C_μ and 0.263 for C_s are obtained, which provide an almost perfect match with the values suggested by the available scientific literature. A more detailed statistical analysis shows that the residuals at the shear layer can be almost perfectly corrected using a global cubic polynomial expression solely dependent on the progress variable \tilde{c} . This fact suggests that the inconsistencies between the baselines models and the observed outputs are mainly caused by chemical aspects. Since a physically motivated

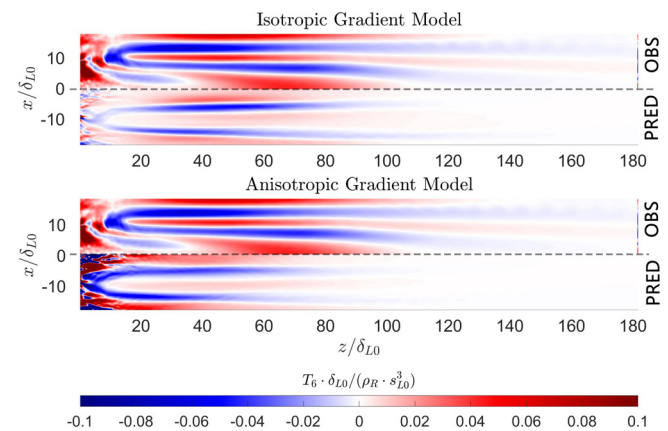


FIG. 15. Observed and predicted values for the term T_6 using the isotropic gradient model in Eq. (36) (top) and the anisotropic gradient model in Eq. (37) (bottom).

model was not found, the results are not reproduced here for the sake of conciseness.

V. CONCLUSIONS

The transport of turbulent kinetic energy in the shear layer of a turbulent diffusion flame has been studied using three-dimensional unsteady direct numerical simulations. Characteristic flame parameters were defined to facilitate the interpretation of flame-turbulence interactions. Definitions for different Damköhler numbers and chemical length scales were proposed. These indicators proved useful to understand the turbulent diffusion flame's behavior. A significant increase in turbulent kinetic energy and its dissipation rate was observed at specific locations. The main contributors for this increase are the turbulence production through mean pressure gradients and the fluctuating pressure gradient terms, which are able to counter the viscous decay throughout most of the reactive shear layer. These mechanisms enhance turbulence through the same mechanisms reported in the scientific literature for turbulent premixed flames at similar conditions. Existing models for premixed combustion were adapted to predict turbulent transport for the pressure-related terms. However, only the novel model for the turbulent production through mean pressure gradients [Eq. (31)] exhibited a good performance both qualitatively and quantitatively. A model of the turbulent transport through fluctuating pressure gradients was proposed as well [Eq. (34)], although with very limited performance. The dissipation rate of turbulent kinetic energy presented a similar behavior compared to what has been observed in premixed flames. The main differences concerning premixed flames were observed in the turbulent transport through pressure gradients [i.e., $\overline{\rho u_i'' u_j''} (\partial \tilde{u}_i / \partial x_i)$], the turbulent molecular viscous transport [i.e., $\nabla(\mu \nabla \tilde{k})$], and the turbulent transport through gradients of the turbulent flux of kinetic energy (i.e., $\overline{\partial \rho u_i'' u_k''^2} / \partial x_i$). Classical gradient models [Eqs. (36) and (37)] were tested to predict this term with moderate success. The inconsistencies of these models are strongly correlated with the progress variable \tilde{c} . This suggests that introducing the interaction between combustion and the shear layer could significantly improve models for the term $\overline{\partial \rho u_i'' u_k''^2} / \partial x_i$.

ACKNOWLEDGMENTS

The authors thank Super-MUC NGen for providing the computational resources for performing the numerical simulations and its post-processing. The authors are extremely grateful to Martin Ohlerich for his support in optimizing the parallel calculations.

AUTHOR DECLARATIONS

Conflict of Interest

The authors have no conflicts of interest to disclose.

DATA AVAILABILITY

The data that support the findings of this study are available from the corresponding author upon reasonable request.

REFERENCES

- ¹B. Karlovitz, D. W. Denniston, and F. E. Wells, "Investigation of turbulent flames," *J. Chem. Phys.* **19**(5), 541–547 (1951).
- ²A. Yoshida and H. Tsuji, "Measurements of fluctuating temperature and velocity in a turbulent premixed flame," *Symp. (Int.) Combust.* **17**, 945 (1979).
- ³K. N. C. Bray, P. A. Libby, G. Masuya, and J. B. Moss, "Turbulence production in premixed turbulent flames," *Combust. Sci. Technol.* **25**(3–4), 127–140 (1981).
- ⁴A. Gulati and J. F. Driscoll, "Flame-generated turbulence and mass fluxes: Effect of varying heat release," *Symp. (Int.) Combust.* **21**, 1367 (1986).
- ⁵D. R. Ballal, "Combustion-generated turbulence in practical combustors," in *23rd Joint Propulsion Conference*, San Diego, CA, 1987.
- ⁶C. J. Rutland and R. S. Cant, "Turbulent transport in premixed flames," in *Proceedings of 1994 Summer Program*, Centre for Turbulence Research, 1994.
- ⁷A. N. Lipatnikov and J. Chomiak, "Effects of premixed flames on turbulence and turbulent scalar transport," *Prog. Energy Combust. Sci.* **36**, 1–102 (2010).
- ⁸V. A. Sabelnikov and A. N. Lipatnikov, "Recent advances in understanding of thermal expansion effects in premixed turbulent flames," *Ann. Rev. Fluid Mech.* **49**, 91–117 (2017).
- ⁹N. Chakraborty, M. Katragadda, and R. S. Cant, "Statistics and modelling of turbulent kinetic energy transport in different regimes of premixed combustion," *Flow, Turbul. Combust.* **87**, 205–235 (2011).
- ¹⁰N. Chakraborty, "Influence of thermal expansion on fluid dynamics of turbulent premixed combustion and its modelling implications," *Flow, Turbul. Combust.* **106**, 753–848 (2021).
- ¹¹O. J. Haidn, M. P. Celano, M. Luo, C. Roth, S. Silvestri, and N. A. Slavinskaya, "On methane/oxygen combustion for rocket applications," in *International Symposium on Innovation and Prospects of Liquid Propulsion*, Xi'an, 2016.
- ¹²D. Maestro, B. Cuenot, A. Chemnitz, T. Sattelmayer, C. Roth, O. J. Haidn, Y. Daimon, R. Keller, G. Frank, M. Pfitzner, and L. Selle, "Numerical investigation of flow and combustion in a single-element GCH₄/GOX rocket combustor: Chemistry modeling and turbulence-combustion interaction," in *52nd AIAA/SAE/ASME Joint Propulsion Conference*, Salt Lake City, UT, 2016.
- ¹³N. Perakis, D. Rahn, O. J. Haidn, and D. Eiringhaus, "Heat transfer and combustion simulation of seven-element O₂/CH₄ rocket combustor," *J. Propul. Power* **35**(1), 1080 (2019).
- ¹⁴S. B. Pope, "The statistical description of turbulent flows," in *Turbulent Flows* (Cambridge University Press, Cambridge, 2000), pp. 34–82.
- ¹⁵M. Eckert, "Chaos and turbulence," in *The Turbulence Problem* (Springer Nature, 2019), pp. 75–85.
- ¹⁶A. Favre, *Problems of Hydrodynamics and Continuum Mechanics* (SIAM, Philadelphia, 1969).
- ¹⁷J. Furukawa, Y. Noguchi, T. Hirano, and F. A. Williams, "Anisotropic enhancement of turbulence in large-scale, low intensity turbulent premixed propane-air flames," *J. Fluid Mech.* **462**, 209–243 (2002).
- ¹⁸J. R. MacDonald and C. M. Fajardo, "Turbulence anisotropy investigations in an internal combustion engine," *J. Eng. Gas Turbines Power* **143**(9), 091011 (2021).
- ¹⁹K. N. C. Bray, "The challenge of turbulent combustion," *Symp. (Int.) Combust.* **26**, 1–26 (1996).
- ²⁰S. B. Pope, "The scales of turbulent motion," in *Turbulent Flows*, Cambridge (Cambridge University Press, 2000), pp. 182–263.
- ²¹S. B. Pope, "Direct numerical simulation," in *Turbulent Flows* (Cambridge University Press, 2000), pp. 344–357.
- ²²P. K. Yeung and S. B. Pope, "Lagrangian statistics from direct numerical simulations of isotropic turbulence," *J. Fluid Mech.* **207**, 531–586 (1989).
- ²³S. Zhang and C. J. Rutland, "Premixed flame effects on turbulence and pressure-related terms," *Combust. Flame* **102**(4), 447–461 (1995).
- ²⁴S. Nishiki, T. Hasegawa, R. Borghi, and R. Himeno, "Modelling of flame-generated turbulence based on direct numerical simulations databases," *Proc. Combust. Inst.* **29**, 2017 (2002).
- ²⁵K. N. C. Bray, P. A. Libby, and J. B. Moss, "Unified modelling approach for premixed turbulent combustion—Part I: General formulation," *Combust. Flame* **61**, 87–102 (1985).
- ²⁶S. B. Pope, "Turbulent-viscosity models," in *Turbulent Flows* (Cambridge University Press, 2000), pp. 358–386.
- ²⁷P. A. Durbin and B. A. Petersson-Reif, *Statistical Theory and Modelling of Turbulent Flows* (Wiley, Hoboken, 2001).
- ²⁸D. C. Wilcox, *Turbulence Modelling for CFD* (DCW, La Cañada, CA, 2002).

- ²⁹Z. Wang and J. Abraham, "Effects of Karlovitz number on turbulent kinetic energy transport in turbulent lean premixed methane/air flames," *Phys. Fluids* **29**, 085102 (2017).
- ³⁰D. Veynante and T. J. Poinso, "Effects of pressure gradients on turbulent premixed flames," *J. Fluid Mech.* **353**, 83–114 (1997).
- ³¹N. Chakraborty and R. S. Cant, "Effects of Lewis number on turbulent scalar transport and its modelling in turbulent premixed flames," *Combust. Flame* **156**, 1427–1444 (2009).
- ³²N. Chakraborty and R. S. Cant, "Physical insight and modelling for Lewis number effects on turbulent heat and mass transport in turbulent premixed flames," *Numer. Heat Transfer A* **55**(8), 762–779 (2009).
- ³³S. Nishiki, T. Hasegawa, R. Borghi, and R. Himeno, "Modelling of turbulent scalar flux in turbulent premixed flames based on DNS databases," *Combust. Theory Modell.* **10**(1), 39–55 (2006).
- ³⁴V. Papapostolou, N. Chakraborty, M. Klein, and H. G. Im, "Statistics of scalar flux transport of major species in different premixed turbulent combustion regimes for H₂-air flames," *Flow, Turbul. Combust.* **102**, 931–955 (2019).
- ³⁵B. L. Launder, G. J. Reece, and W. J. Rodi, "Progress in the development of a Reynolds stress turbulence closure," *J. Fluid Mech.* **68**, 537–566 (1975).
- ³⁶P. Domingo and K. N. C. Bray, "Laminar flamelet expressions for pressure fluctuation terms in second moment models of premixed turbulent combustion," *Combust. Flame* **121**, 555–574 (2000).
- ³⁷D. Martínez-Sanchis, A. Sternin, K. Tagscherer, D. Sternin, O. Haidn, and M. Tajmar, "Interactions between flame topology and turbulent transport in high-pressure premixed combustion," (unpublished).
- ³⁸L. Vervisch and T. Poinso, "Direct numerical simulation of non-premixed turbulent flames," *Annu. Rev. Fluid Mech.* **30**, 655–691 (1998).
- ³⁹C. K. Law, "Conservation equations," in *Combustion Physics* (Cambridge University Press, 2006), pp. 157–193.
- ⁴⁰B. Cuenot, "The flamelet model for non-premixed combustion," in *Turbulent Combustion Modelling* (Springer Nature, 2011), pp. 43–61.
- ⁴¹A. Najafi-Yazdi, B. Cuenot, and L. Mongeau, "Systematic definition of progress variables and intrinsically low-dimensional, flamelet generated manifolds for chemistry tabulation," *Combust. Flame* **159**, 1197–1204 (2012).
- ⁴²K. Bray, P. Domingo, and L. Vervisch, "Role of the progress variable in models for partially premixed turbulent combustion," *Combust. Flame* **141**(4), 431–437 (2005).
- ⁴³N. Peters, *Turbulent Combustion* (Cambridge University Press, Cambridge, 2001).
- ⁴⁴R. W. Bilger, "Turbulent jet diffusion flames," *Prog. Energy Combust. Sci.* **1**(2–3), 87–109 (1976).
- ⁴⁵C. D. Pierce and P. Moin, "Progress-variable approach for large-eddy simulation of non-premixed turbulent combustion," *J. Fluid Mech.* **504**, 73–97 (2004).
- ⁴⁶T. Zirwes, F. Zhang, P. Habisreuther, M. Hansinger, H. Bockhorn, M. Pfitzner, and D. Trimis, "Identification of flame regimes in partially premixed combustion from a quasi-DNS dataset," *Flow, Turbul. Combust.* **1006**, 373–404 (2021).
- ⁴⁷T. Seitz, A. Lechtenberg, and P. Gerlinger, "Rocket combustion chamber simulations using high-order methods," in *Future Space-Transport-System Components under High Thermal and Mechanical Loads* (Springer Professional, 2011), pp. 381–394.
- ⁴⁸P. H. Joo, M. R. J. Charest, C. P. T. Groth, and Ö. L. Gülder, "Comparison of structures of laminar methane-oxygen and methane-air diffusion flames from atmospheric to 60 atm," *Combust. Flame* **160**(1), 1990–1998 (2013).
- ⁴⁹T. Poinso and D. Veynante, "Turbulent non premixed flames," in *Theoretical and Numerical Combustion* (Bordeaux, France, 2012), pp. 287–348.
- ⁵⁰A. M. Kanury, *Introduction to Combustion Phenomena* (Gordon and Breach Science Publisher, New York, 1975).
- ⁵¹M. Katragada, N. Chakraborty, and R. S. Cant, "A priori assessment of algebraic flame surface density models in the context of large eddy simulation for nonunity Lewis number flames in the thin reaction zones regime," *J. Combust.* **2012**, 794671.
- ⁵²A. Trounev and T. Poinso, "The evolution equation for the flame surface density in turbulent premixed combustion," *J. Fluid Mech.* **278**, 1–31 (1994).
- ⁵³S. B. Pope, "The evolution of surfaces in turbulence," *Int. J. Eng. Sci.* **26**(5), 445–469 (1988).
- ⁵⁴A. Liñán, "The asymptotic structure of counterflow diffusion flames for large activation energies," *Acta Astronaut.* **1**(7–8), 1007–1039 (1974).
- ⁵⁵D. O. Lignell, J. H. Chen, and H. A. Schmutz, "Effects of Damköhler number on flame extinction and reignition in turbulent non-premixed flames using DNS," *Combust. Flame* **158**, 949–963 (2011).
- ⁵⁶B. Cuenot and T. Poinso, "Effects of curvature and unsteadiness in diffusion flames. Implications for turbulent diffusion combustion," *Symp. (Int.) Combust.* **25**(1), 1383–1390 (1994).
- ⁵⁷D. Martínez-Sanchis, A. Sternin, D. Sternin, O. Haidn, and M. Tajmar, "Analysis of periodic synthetic turbulence generation and development for direct numerical simulations applications," *Phys. Fluids* **33**, 125130 (2021).
- ⁵⁸M. L. Shur, P. R. Spalart, M. K. Strelets, and A. K. Travin, "Synthetic turbulence generators for RANS-LES interfaces in zonal simulations of aerodynamic and aeroacoustic problems," *Flow, Turbul. Combust.* **93**, 63–92 (2014).
- ⁵⁹R. H. Kraichnan, "Diffusion by a random velocity field," *Phys. Fluids* **13**, 22–31 (1970).
- ⁶⁰A. Sternin, N. Perakis, M. P. Celano, and O. Haidn, "CFD-analysis of the effect of a cooling film on flow and heat transfer characteristics in a GCH₄/GOX rocket combustion chamber," in *Space Propulsion*, Sevilla, 2018.
- ⁶¹F. Zhang, H. Bonart, T. Zirwes, and P. Habisreuther, "Direct numerical simulations of chemically reacting flows with the public domain code OpenFOAM," in *High Performance Computing in Science and Engineering '16* (Springer, 2015), pp. 221–236.
- ⁶²T. Zirwes, F. Zhang, J. Denev, P. Habisreuther, and H. Bockhorn, "Automated code generation for maximizing performance of detailed chemistry calculations in OpenFOAM," in *High Performance Computing in Science and Engineering '17* (Springer, 2018), pp. 189–204.
- ⁶³T. Zirwes, F. Zhang, J. A. Denev, P. Habisreuther, H. Bockhorn, and D. Trimis, "Improved vectorization for efficient chemistry computations in OpenFOAM for large scale combustion simulations," in *High Performance Computing in Science and Engineering '18* (Springer, 2019), pp. 209–224.
- ⁶⁴T. Zirwes, F. Zhang, P. Habisreuther, J. A. Denev, H. Bockhorn, and D. Trimis, "Implementation and validation of a computationally efficient DNS solver for reacting flows in OpenFOAM," in *14th World Congress on Computational Mechanics* (Virtual Congress, 2021).
- ⁶⁵H. Weller, G. Tabor, H. Jasak, and C. Fureby, "A tensorial approach to computational continuum mechanics using object-oriented techniques," *Computers Phys.* **12**(6), 620–631 (1998).
- ⁶⁶H. Weller, G. Tabor, H. Jasak, and C. Fureby, *OpenFOAM* (OpenCFD Ltd, 2017).
- ⁶⁷P. W. McDonald, "The computation of transonic flow through two-dimensional gas turbine cascades," in *International Gas Turbine Conference and Products Show*, 1971.
- ⁶⁸R. W. MacCormack and A. J. Paullay, "Computational efficiency achieved by time splitting of finite difference operators," in *10th Aerospace Sciences Meeting*, San Diego, 1972.
- ⁶⁹F. Zhang, T. Zirwes, H. Nawroth, P. Habisreuther, H. Bockhorn, and C. O. Paschereit, "Combustion-generated noise: An environment-related issue for future combustion systems," *Energy Technol.* **5**, 1045–1054 (2017).
- ⁷⁰F. Zhang, T. Zirwes, P. Habisreuther, and H. Bockhorn, "Effect of unsteady stretching on the flame local dynamics," *Combust. Flame* **175**, 170–179 (2017).
- ⁷¹T. Zirwes, T. Häber, Z. Feichi, H. Kosaka, A. Dreizler, M. Steinhausen, C. Hasse, A. Stagni, D. Trimis, R. Suntz, and H. Bockhorn, "Numerical study of quenching distances for side-wall quenching using detailed diffusion and chemistry," *Flow, Turbul. Combust.* **106**, 649–679 (2021).
- ⁷²F. Zhang, T. Zirwes, T. Häber, H. Bockhorn, D. Trimis, and R. Suntz, "Near wall dynamics of premixed flames," *Proc. Combust. Inst.* **38**, 1955–1964 (2020).
- ⁷³T. Zirwes, F. Zhang, P. Habisreuther, M. Hansinger, H. Bockhorn, M. Pfitzner, and D. Trimis, "Quasi-DNS dataset of a piloted flame with inhomogeneous inlet conditions," *Flow, Turbul. Combust.* **104**, 997–1027 (2020).
- ⁷⁴D. Goodwin, H. Moffat, and R. Speth, "Cantera: An object-oriented software toolkit for chemical kinetics, thermodynamics and transport processes version 2.3.0b," (2015); available at <http://www.cantera.org>.
- ⁷⁵R. Kee, M. Coltrin, and P. Glarborg, *Chemically Reacting Flow: Theory and Practice* (Wiley, London, 2005).
- ⁷⁶N. Slavinskaya, M. Abbasi, J. H. Starcke, and O. Haidn, "Methane skeletal mechanism for space propulsion applications," in *Joint Propulsion Conference*, Salt Lake City, UT, 2016.

- ⁷⁷T. Poinso and D. Veynante, "Introduction to turbulent combustion," in *Theoretical and Numerical Combustion* (R. T. Edwards, Inc., 2005), pp. 125–181.
- ⁷⁸J. Jeong and F. Hussain, "On the identification of a vortex," *J. Fluid Mech.* **285**, 69–94 (1995).
- ⁷⁹P. N. Kioni, B. Rogg, K. N. C. Bray, and A. Liñán, "Flame spread in laminar mixing layers: The triple flame," *Combust. Flame* **95**(3), 276–290 (1993).
- ⁸⁰D. Veynante, L. Vervisch, T. Poinso, and A. R. G. Liñán, "Triple flame structure and diffusion flame stabilization," in Center for Turbulence Research, Proceedings of the Summer Program, 1994.
- ⁸¹J. F. MacArt, T. Grenga, and M. E. Mueller, "Effects of combustion heat release on velocity and scalar statistics in turbulent premixed jet flames at low and high Karlovitz numbers," *Combust. Flame* **191**, 468–485 (2018).
- ⁸²S. Candel, D. Veynante, F. Lacas, E. Maistret, N. Darabiha, and T. Poinso, "Coherent flame model: Applications and recent extensions," in *Advances in Combustion Modelling* edited by B. Larrouturou (CERMICS, INRIA Sophia-Antipolis, Singapore, 1990), pp. 19–64.
- ⁸³N. Darabiha, V. Giovangigli, A. Trouvé, S. M. Candel, and E. Esposito, "Coherent flame description of turbulent premixed ducted flames," in *Turbulent Reacting Flows, Lecture Notes in Engineering* (Springer, 1987), pp. 591–637.
- ⁸⁴R. S. Cant, S. B. Pope, and K. N. C. Bray, "Modelling of flamelet surface to volume ratio in turbulent premixed combustion," in 23rd Symposium International on Combustion, Pittsburgh, 1990.
- ⁸⁵B. J. Daly and F. H. Harlow, "Transport equations in turbulence," *Phys. Fluids* **13**, 2634–2649 (1970).